

# Nonlocal control of pulse propagation in excitable media

Clemens A. Bachmair and Eckehard Schöll

Institut für Theoretische Physik, Technische Universität Berlin, 10623 Berlin, Germany

Received: date / Revised version: date

**Abstract** We study the effects of nonlocal control of pulse propagation in excitable media. As a generic example for an excitable medium the FitzHugh-Nagumo model with diffusion in the activator variable is considered. Nonlocal coupling in form of an integral term with a spatial kernel is added. We find that the nonlocal coupling modifies the propagating pulses of the reaction-diffusion system such that a variety of spatio-temporal patterns are generated including acceleration, deceleration, suppression, or generation of pulses, multiple pulses, and blinking pulse trains. It is shown that one can observe these effects for various choices of the integral kernel and the coupling scheme, provided that the control strength and spatial extension of the integral kernel is appropriate. In addition, an analytical procedure is developed to describe the stability borders of the spatially homogeneous steady state in control parameter space in dependence on the parameters of the nonlocal coupling.

**PACS.** 05.45.-a, 05.65.+b, 82.40.Ck

## 1 Introduction

Excitable media in the form of nonlinear reaction-diffusion systems are used to model a wide range of physical, chemical, biological, as well as socio-economic phenomena [17, 26, 37, 20, 22]. For certain parameter ranges they support traveling excitation pulses. An important application in neuroscience is the propagation of information along a nerve fiber. Excitation pulses in the form of spreading depression or depolarization are also associated with pathological states of brain activity occurring, for instance, during migraine or stroke [21, 13, 10]. If, in addition to local diffusion, nonlocal spatial coupling is present, this represents an important internal control mechanism in neuronal wave dynamics. The resulting spatio-temporal patterns in nonlocally coupled reaction-diffusion systems can be quite complex, ranging from traveling waves, Turing patterns, and pulse trains to spatio-temporal chaos [4, 33, 49, 18, 28, 41, 54, 40, 6, 8, 15, 30]. Such nonlocal couplings in the form of integrals with a spatial kernel can be derived as limiting cases of two- or three-component activator-inhibitor reaction-diffusion models with or without advection, when fast inhibitor variables are eliminated adiabatically [44, 43, 41, 52, 50, 51]. In particular, asymmetric spatial kernels [51] arise from differential advection of some chemical species, e.g., in heterogeneous catalysis, marine biology, or ecology [36, 57, 46, 23, 31, 55]. In the limit of global spatial coupling, i.e., fast diffusion of the eliminated variable, a large number of experimental and theoretical studies, e.g., in the CO oxidation on platinum surfaces [3, 5] and other catalytic processes [36], as well as in electrochemistry [45] or in semiconductors [35, 48] have shown that global feedback can control propagating waves and generate spatially pe-

riodic patterns such as Turing patterns or travelling waves [38]. In electrochemistry, models with explicit nonlocal coupling have been derived from more elementary models by applying a Green's function formalism, see e.g. [7]. Nonlocal coupling plays also an essential role in the formation of chimera states in systems of coupled oscillators [27, 1, 16, 53, 32, 42, 58].

In neuronal systems, especially in the visual cortex, several experimental studies have given evidence for nonlocal long-range connectivity of neurons [19, 56]. In the framework of the FitzHugh-Nagumo model of excitable dynamics augmented by a spatially discrete nonlocal coupling term, it was shown that traveling pulses in one spatial dimension can be suppressed by various control schemes of spatially nonlocal or time-delayed coupling [12, 47]. This has been explained by the effective change of the excitation threshold of the original reaction-diffusion system by nonlocal interaction at a certain spatial distance and a certain coupling strength. The nucleation and propagation of spatially localized reaction-diffusion waves has also been studied in two-dimensional flat [11] and curved surfaces [24] under global spatial feedback in the framework of the FitzHugh-Nagumo model. In particular, it was shown that the stability of propagating wave segments depends crucially on the curvature of the surface [24].

Here we extend the results on one-dimensional pulse propagation in the FitzHugh-Nagumo model by a systematic study of spatially continuous nonlocal couplings with different integral kernels, including Mexican hat kernels which are of particular relevance for interacting cortical neurons since they combine excitatory coupling of neighbouring cells with long-range inhibitory interactions

of distant cells [19]. We show that the resulting spatio-temporal patterns can be acceleration, deceleration, and suppression of propagating pulses as well as generation of Turing patterns, and multiple pulses and blinking traveling waves. The organization of the paper is as follows. In section 2 we introduce the FitzHugh-Nagumo model with nonlocal coupling. In section 3 a linear stability analysis of the homogeneous steady state is performed, which gives rise to various spatio-temporal instabilities. In section 4 we present simulations of the nonlinear reaction-diffusion equations with different nonlocal kernels, and discuss the resulting complex patterns.

## 2 FitzHugh-Nagumo model with nonlocal coupling

In this paper an excitable medium is modeled by the generic FitzHugh-Nagumo (FHN) system [14, 39, 29] which is spatially extended in one dimension by diffusion only in the activator variable:

$$\dot{u} = u - \frac{u^3}{3} - v + \partial_{xx}u, \quad (1)$$

$$\epsilon^{-1}\dot{v} = u + \beta, \quad (2)$$

where  $u$  and  $v$  denote the activator (membrane potential) and the inhibitor (recovery variable), respectively,  $0 < \epsilon \ll 1$  separates the time scale of the fast activator  $u$  and the slow inhibitor  $v$ , and  $\beta$  is an indicator for the excitability of the system. The diffusion constant is scaled to unity. In the excitable regime ( $\beta > 1$ ) there exists a stable homogeneous steady state. These equations show – for appropriate values of  $\epsilon$  and  $\beta$  – the well-known behavior of supporting traveling pulses and waves after supra-threshold excitations. Throughout this paper we use the parameters  $\epsilon = 0.08$  and  $\beta = 1.2$ . The spatially homogeneous steady state is given by:

$$(u^*, v^*)^T = \left( -\beta, \frac{\beta^3}{3} - \beta \right)^T. \quad (3)$$

Now a nonlocal control term  $\hat{K}$  is added to the system Eqs. (1) and (2). Introducing the vector notation  $U = (u, v)^T$  we can write the nonlocally coupled FHN system as:

$$E\dot{U} = F(U) + \hat{D}U + \hat{K}U, \quad (4)$$

where

$$E = \begin{pmatrix} 1 & 0 \\ 0 & \epsilon^{-1} \end{pmatrix}, \quad (5)$$

is the time scale separation matrix,  $F(U)$  describes the FHN dynamics given by the right hand sides of Eqs. (1),(2), and

$$\hat{D} = \begin{pmatrix} \partial_{xx} & 0 \\ 0 & 0 \end{pmatrix}, \quad (6)$$

is the diffusion matrix. The nonlocal control operator  $\hat{K}$  is defined as follows:

$$\hat{K}U = \kappa A \left[ \int U(x - x') \ker(x') dx' - \eta U(x) \right], \quad (7)$$

where  $\kappa \in \mathbb{R}$  is the control strength,  $A \in \mathbb{R}^{2 \times 2}$  is a  $2 \times 2$  coupling matrix, which may be chosen, e.g., as one of the following:

$$\begin{aligned} A^{uu} &= \begin{pmatrix} 1 & 0 \\ 0 & 0 \end{pmatrix}, & A^{uv} &= \begin{pmatrix} 0 & 1 \\ 0 & 0 \end{pmatrix}, \\ A^{vu} &= \begin{pmatrix} 0 & 0 \\ 1 & 0 \end{pmatrix}, & A^{vv} &= \begin{pmatrix} 0 & 0 \\ 0 & 1 \end{pmatrix}, \end{aligned} \quad (8)$$

where the superscripts label the coupling scheme, e.g.,  $A^{uu}$  denotes a matrix representing the coupling scheme  $uu$ . The function  $\ker(x)$  is an integral kernel satisfying:

$$\ker(x) = \ker(-x), \quad \int_{-\infty}^{\infty} |\ker(x)| dx = 1.$$

The term

$$\eta U(x) = \int \ker(x') dx' U(x) \quad (9)$$

in Eq. (7) is introduced in order to make the control noninvasive with respect to the homogeneous steady state, i.e., the homogeneous steady state is not changed by the control term  $\hat{K}U$ . In this paper we will focus on the following three symmetric integral kernels:

$$\ker(x) = \frac{1}{2} (\delta(x + \sigma) + \delta(x - \sigma)), \quad (10)$$

$$\ker(x) = \frac{1}{2\sigma} e^{-\frac{|x|}{\sigma}}, \quad (11)$$

$$\ker(x) = \frac{N}{\sigma\sqrt{2\pi}} \left( \frac{1}{r} e^{-\frac{x^2}{2(r\sigma)^2}} - e^{-\frac{x^2}{2\sigma^2}} \right), \quad 0 < r < 1, \quad (12)$$

where  $\sigma$  is a characteristic nonlocal coupling range, and  $r = \sigma_e/\sigma_i < 1$  describes the ratio of short-range excitatory ( $\sigma_e$ ) and long-range inhibitory ( $\sigma_i$ ) interaction in the Mexican hat kernel Eq. (12). The prefactor  $N$  is chosen such that the kernel in Eq. (12) is normalized in the  $L_1$  norm. For the  $\delta$ -function Eq. (10) and the exponential kernel Eq. (11)  $\eta = 1$  (to secure noninvasiveness), while for the Mexican hat kernel Eq. (12)  $\eta = 0$ . Figure 1 shows plots of these kernels, and additionally an anisotropic  $\delta$ -function kernel  $\ker(x) = \delta(x + \sigma)$  (corresponding to backward coupling only) and a rectangular kernel which simplifies to the symmetric  $\delta$ -function kernel in the limit of zero width  $w$ .

The system (4) has been analyzed by Schneider et al. for isotropic (symmetric) and anisotropic (asymmetric)  $\delta$ -function integral kernels [47]. They have shown that the control scheme can be used to suppress excitation pulses for appropriate control parameters. We will extend this work in three directions. First of all, we also consider spatially extended integral kernels such as the exponential and the Mexican hat function. It has been shown that the adiabatic elimination of a fast variable in a three-variable system results in a nonlocal integral term that has the form of an exponential kernel [50], see also [51]. Second, nonlocal control does not only suppress propagating pulses but can also be used to accelerate or decelerate pulses as well as to generate pulses or wave trains. We will

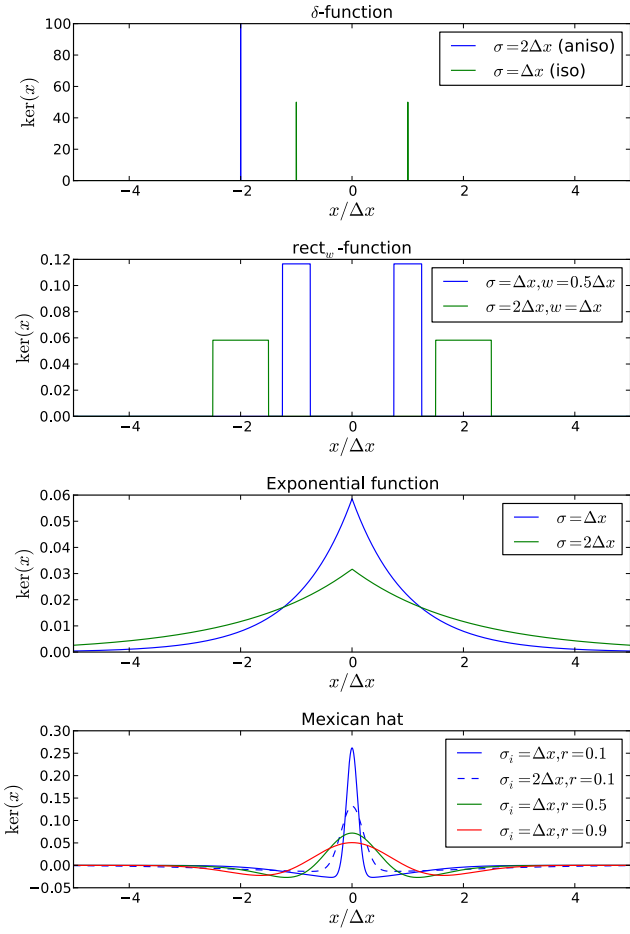


Figure 1: Various nonlocal control kernels  $\ker(x)$ , see Eqs. (7),(10)-(12), for different characteristic interaction lengths  $\sigma$ . The length is scaled in units of  $\Delta x = 8.59$  which is the pulse width of the uncontrolled pulse for  $(\varepsilon, \beta) = (0.08, 1.2)$ . The anisotropic  $\delta$ -function (top panel, labeled *aniso*) corresponds to backward coupling for a pulse traveling in positive  $x$ -direction.

take these effects into account and explore the phase diagrams in control parameter space showing where to expect which kind of behavior. Finally, we will gain some analytical insights by analyzing the stability of the homogeneous steady state, and determining how its stability is affected by nonlocal control. We show that the control scheme enables the generation of a plethora of different instabilities.

### 3 Stability analysis

Before investigating the effects of the control upon a traveling pulse, we will focus on the instabilities of the homogeneous steady state (HSS) first. This will allow us to get some analytical insight. After a survey of the possible spatio-temporal instabilities in excitable media we will analytically describe the stability borders in the control pa-

rameter space of the control strength  $\kappa$  and the nonlocal coupling range  $\sigma$ .

#### 3.1 Instabilities of the homogeneous steady state

Generally, the stable homogeneous steady state of a spatially extended system can become unstable by different spatio-temporal bifurcations when the control parameters are changed. We characterize the different instabilities by the behavior of the dispersion relation obtained from a linear stability analysis of the homogeneous steady state, i.e., the eigenvalue  $\Lambda(k)$  in dependence upon the wavenumber  $k$ . Depending upon the value  $k_c$  at which the bifurcation ( $\text{Re } \Lambda(k_c) = 0$ ) occurs and the corresponding imaginary part of the eigenvalue  $\text{Im } \Lambda(k_c)$ , four different cases can be distinguished: (i) A Hopf instability causing spatially homogeneous oscillations occurs for  $k_c = 0$  and  $\text{Im } \Lambda(k_c) \neq 0$ . (ii) A Turing instability is given when  $k_c \neq 0$  and  $\text{Im } \Lambda(k_c) = 0$ , which leads to a stationary spatial modulation. (iii) A wave instability is characterized by  $k_c \neq 0$  and  $\text{Im } \Lambda(k_c) \neq 0$ . Both (ii) and (iii) have in common that upon further increase of the bifurcation parameter there appears a finite interval of unstable wavenumbers  $[k_-, k_+]$ :

$$\text{Re } \Lambda(k) > 0 \quad \forall |k| \in [k_-, k_+], \quad (13)$$

(iv) If the instability  $\text{Re } \Lambda(k_c) = 0$  occurs at  $k_c \rightarrow \infty$ , the condition (13) is not fulfilled. Rather, the following degenerate case holds upon further increase of the bifurcation parameter beyond the bifurcation:

$$\text{Re } \Lambda(k) > 0 \quad \forall |k| > k_0, \quad (14)$$

Thus arbitrarily large wavenumbers become unstable, which can cause patterns with arbitrarily short wavelengths. Such instabilities have been called *salt-and-pepper patterns* [25], and it has been suggested that they might occur in morphogenesis when differentiated cells inhibit the differentiation of neighboring cells, as is seen, for example, with differentiated neuroprogenitor cells in the epithelium of Drosophila embryos [25]. Figure 2 illustrates the difference of the Turing or wave instability (upper panel) and the salt-and-pepper instability (lower panel). A tabular overview of the instabilities (i)-(iv) is given in Table 1. Three examples of the spatio-temporal patterns generated by the instabilities (ii)-(iv) are provided in Figure 3 from simulations of the full nonlinear equations (4). After some initial transients a wave instability (a), a Turing instability (b), and a salt-and-pepper instability (c) develops. In each case the initial condition at  $t = 0$  is the homogeneous steady state to which Gaussian white noise is added. Fig. 4 shows schematically the space-time patterns corresponding to the instabilities (i) - (iii) of the homogeneous steady state in reaction-diffusion systems: Hopf, Turing, wave train; additionally, the pattern on the very right corresponds to a combined Turing-Hopf codimension-two instability [34].

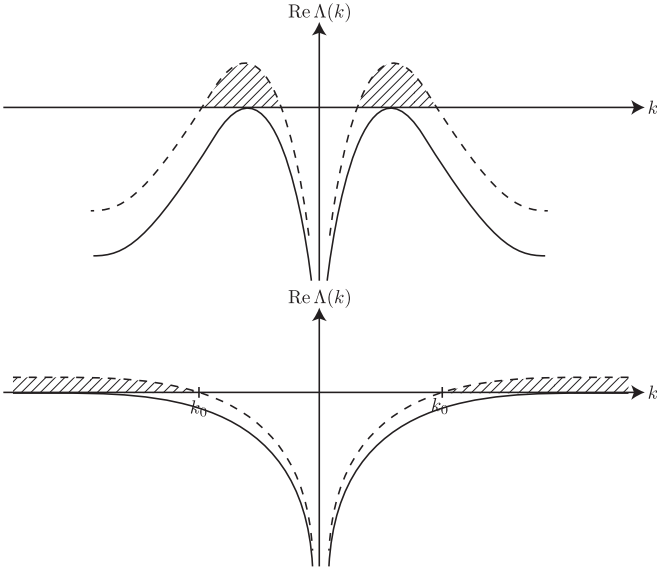


Figure 2: Schematic dispersion relation of the homogeneous steady state for Turing or wave instability (top) and salt-and-pepper instability (bottom). The solid and dashed lines mark  $\text{Re } \Lambda(k)$  at the bifurcation point and beyond the bifurcation, respectively. The hatched region corresponds to the band of unstable wavevectors beyond the bifurcation.

Table 1: Instabilities of the homogeneous steady state that give rise to pattern formation in reaction-diffusion systems

Instability	$ k_c $	$\text{Im } \Lambda(k_c)$
Hopf	0	$\neq 0$
Turing	$\neq 0$ , finite	$= 0$
Wave	$\neq 0$ , finite	$\neq 0$
Salt-and-pepper	infinite; $\exists k_0 : \text{Re } \Lambda^+(k) > 0 \quad \forall  k  > k_0$	--

### 3.2 Stability boundaries in control parameter space

We can obtain an analytical expression for the stability boundaries of the homogeneous steady state in control parameter space  $(\kappa, \sigma)$  with the help of a linear stability analysis. We linearize the system (4) about the homogeneous steady state  $U_{\text{hom}}^*$  for small perturbations  $\delta U$ . The resulting linear differential equation can be solved with the ansatz  $\delta U \sim e^{\Lambda t} e^{ikx}$ , which yields the following characteristic equation:

$$0 = \det \begin{bmatrix} \Lambda + b(k) & 1 \\ -1 & \varepsilon^{-1} \Lambda \\ -\kappa A(\tilde{g}(k) - \eta) \end{bmatrix}, \quad (15)$$

where  $b(k) = k^2 + \beta^2 - 1 > 0$  and  $\tilde{g}$  is the Fourier transform of the integral kernel:

$$\tilde{g}(k) = \int_{-\infty}^{\infty} \text{ker}(x) e^{-ikx} dx. \quad (16)$$

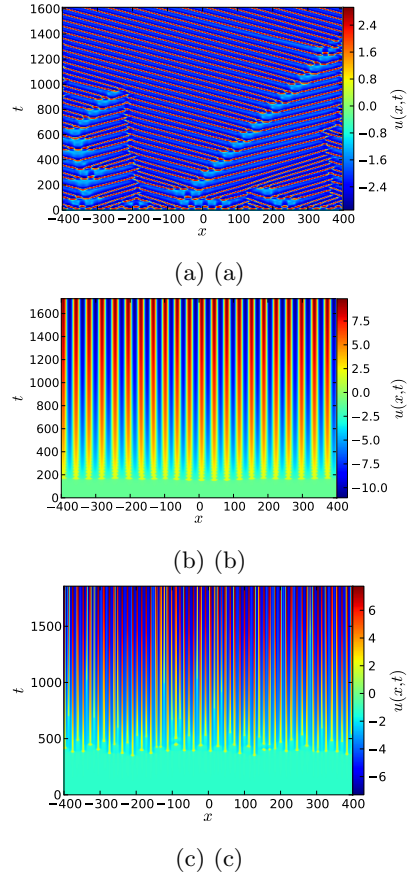


Figure 3: Space-time plots of the onset of spatio-temporal instabilities of the homogeneous steady state caused by nonlocal control. As initial condition weak white noise is added to the homogeneous steady state. The control is switched on at  $t = 0$ . (a) Wave instability: Mexican hat kernel,  $uv$ -coupling-scheme,  $r = \sigma_e/\sigma_i = 0.9$ ,  $(\kappa, \sigma_i) = (1.5, \Delta x)$ , (b) Turing instability: Mexican hat kernel,  $uv$ -coupling-scheme,  $r = \sigma_e/\sigma_i = 0.9$ ,  $(\kappa, \sigma_i) = (1.75, \Delta x)$ , (c) Salt-and-pepper instability: Exponential kernel,  $uv$ -coupling-scheme,  $(\kappa, \sigma) = (-1.25, 2\Delta x)$ . Parameters:  $\varepsilon = 0.08$ ,  $\beta = 1.2$ ,  $L = 800$ , simulation timestep  $dt = 0.005$ .

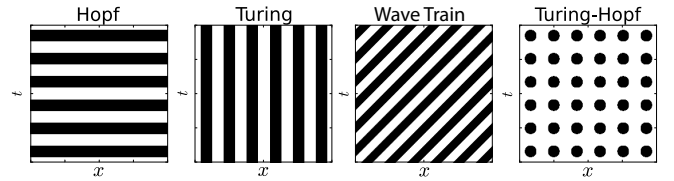


Figure 4: Schematic space-time patterns in reaction-diffusion systems corresponding to the instabilities of the homogeneous steady state: Hopf, Turing, wave train, Turing-Hopf (from left to right).

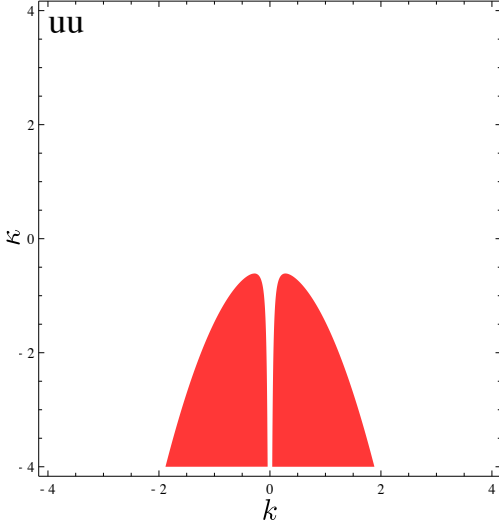


Figure 5: Stability regimes of the homogeneous steady state. Red indicates control parameters  $(\kappa, \sigma)$  destabilizing the homogeneous steady state. Control parameters:  $\sigma = \Delta x$ , exponential kernel,  $uu$  coupling scheme. System parameters:  $\varepsilon = 0.08, \beta = 1.2$ .

For further analytical progress we need to specify the coupling scheme. Here we will present the calculations for the activator self-coupling scheme  $\mathbf{A}^{uu}$  and the exponential integral kernel. Similar results have been obtained for the other coupling schemes and integral kernels [2]. The characteristic equation (15) reads for the  $uu$ -coupling scheme:

$$\Lambda^2 + \Lambda(b(k) - \kappa(\tilde{g}(k) - \eta)) + \varepsilon = 0 \quad (17)$$

which yields the dispersion relation

$$\Lambda_{\pm}(k) = \frac{1}{2} \left\{ -b(k) + \kappa(\tilde{g}(k) - \eta) \pm \sqrt{[b(k) - \kappa(\tilde{g}(k) - \eta)]^2 - 4\varepsilon} \right\}. \quad (18)$$

For a given control configuration we determine the stability of the homogeneous steady state by calculating the maximum real part of  $\Lambda_+(k)$ , as  $\text{Re}(\Lambda_+) > \text{Re}(\Lambda_-)$ . Let us assume that a control configuration consisting of the coupling scheme  $A$ , the integral kernel  $\text{ker}(x)$  with the coupling range  $\sigma_0$ , and the coupling strength  $\kappa_0$  are given. This configuration destabilizes the homogeneous steady state if

$$\exists k \in \mathbb{R} : \mu = \max \text{Re}(\Lambda_{\pm}(k)) > 0. \quad (19)$$

In Fig. 5, the stability of the homogeneous steady state is calculated numerically for the exponential kernel in the  $uu$ -coupling scheme for  $\sigma = \Delta x$ . The control strength  $\kappa$  is varied and so is the wavenumber  $k$ . Regimes with an unstable homogeneous steady state are colored red. There is a critical control strength  $\kappa_c(\sigma) = -0.61$ . For  $\kappa < \kappa_c$  the control destabilizes the homogeneous steady

state, whereas the stability of the homogeneous steady state is not affected for  $\kappa > \kappa_c$ . The critical wave number  $k_c$  is the key to the analytical description of the stability border in control parameter space  $(\kappa, \sigma)$ . The stability border is described by the set of control parameters  $(\kappa, \sigma)$  for which we can find a  $k$  fulfilling:

$$\text{Re}(\Lambda_+(k)) = 0, \quad (20)$$

$$\partial_k \text{Re}(\Lambda_+(k)) = 0. \quad (21)$$

Using Eq. (20) we obtain a closed analytical expression:

$$\kappa = \frac{b(k)}{\tilde{g}(k) - \eta}. \quad (22)$$

Substitution into Eq. (21) gives:

$$-2k + b(k) \frac{\partial_k \tilde{g}(k)}{\tilde{g}(k) - \eta} = 0. \quad (23)$$

Using Eq. (23) and substituting  $\tilde{g}(k) = (1 + k^2 \sigma^2)^{-1}$  and  $\eta = 1$  for the exponential kernel we find:

$$k_c = \sqrt[4]{\frac{\beta^2 - 1}{\sigma^2}}, \quad (24)$$

which gives us the stability border together with Eq. (22):

$$\sigma(\kappa) = \frac{1}{\sqrt{-\kappa} - \sqrt{\beta^2 - 1}}, \quad (25)$$

where  $\kappa < 1 - \beta^2$  as  $k_c \in \mathbb{R}$ :

$$k_c = \pm \sqrt[4]{a} \sqrt{\sqrt{-\kappa} - \sqrt{\beta^2 - 1}}. \quad (26)$$

Thus, we have found an analytical expression for the stability boundary in control parameter space  $(\kappa, \sigma)$ . As the critical wavenumber  $k_c \neq 0$ , the emerging instability is either a Turing, a wave, or a salt-and-pepper instability. The latter can be excluded because of the following asymptotic behavior for large  $k$ :

$$\text{Re} \Lambda_+(k \gg 1) = \Lambda_+(k) = -\frac{\varepsilon}{k^2} + \mathcal{O}(k^{-4}) < 0. \quad (27)$$

This result implies that we cannot find a  $k_0$  fulfilling Eq. (14) and, thus, we can exclude the salt-and-pepper instability for this type of kernel and coupling scheme.

## 4 Simulation of pulses

The system given by Eq. (4) is simulated for a wide range of parameters for four different coupling schemes with the three control kernels presented in Eqs. (10)-(12). The initial condition is the stable traveling pulse that forms after an excitation of the uncontrolled system. In all simulations the boundary conditions are periodic. The diffusion is implemented with the spectral method [9]. At time  $t = 0$  the control is switched on. For every parameter configuration, the effect of the control term is classified as one of the following:

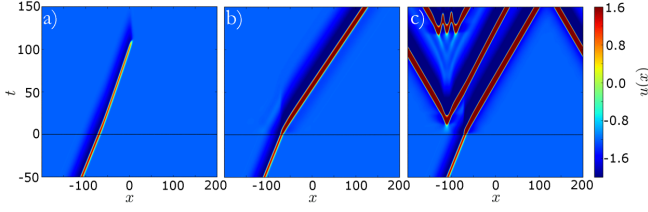


Figure 6: Classification of the effects of the nonlocal control on a traveling pulse. The control is switched on at  $t = 0$ . (a) Exponential kernel,  $vv$ -coupling-scheme,  $(\kappa, \sigma_i) = (0.5, 0.275\Delta x)$ , (b) Mexican hat kernel,  $uu$ -coupling-scheme,  $r = \sigma_e/\sigma_i = 0.1$ ,  $(\kappa, \sigma_i) = (0.5, 2\Delta x)$ , (c) Exponential kernel,  $uu$ -coupling-scheme,  $(\kappa, \sigma_i) = (-0.75, 1.5\Delta x)$ . Parameters:  $(\varepsilon, \beta) = (0.08, 1.20)$ .

- (a) Pulse suppression,
- (b) Pulse acceleration or deceleration,
- (c) Multiple pulse generation.

Examples of spatiotemporal plots for each class are provided in Fig. 6. Panel (a) shows pulse suppression, (b) shows pulse acceleration, and (c) shows the generation of a pair of pulses propagating into opposite directions. Figs. 7-9 summarize the results for the different regimes in the  $(\kappa, \sigma)$  control parameter plane for the four coupling schemes and the  $\delta$ -function kernel (Fig. 7), the exponential kernel (Fig. 8), and the Mexican hat kernel (Fig. 9). In addition, the analytically calculated stability boundary of the homogeneous steady state is plotted.

#### 4.1 Isotropic $\delta$ -function kernel

In the  $uu$ -coupling scheme (Fig. 7, top left), pulse suppression (PS) can only be achieved with positive control strength  $\kappa$ . This is in accordance with [47]. For negative control strength there is a large regime of multiple pulse (MP) generation. The border to this regime is well described by the analytically calculated stability boundary of the homogeneous steady state. The corresponding instability (diagonal hatching) is a wave instability. For small  $\sigma$  and positive  $\kappa$  the pulse is accelerated (green), while for small  $\sigma$  and negative  $\kappa$  the pulse is slowed down (violet and blue). This behavior changes when  $\sigma$  is increased.

The  $uv$ - (top right) and  $vu$ -coupling schemes (bottom left) are related to each other by an approximate reflection symmetry with respect to  $\kappa \rightarrow -\kappa$ , at least for not too large  $\sigma$ , and thus they show qualitatively similar behavior. Pulse suppression can be achieved for negative and positive control strengths. In case of  $uv$ - ( $vu$ -)coupling, the stability boundary of the homogeneous steady state is described by  $\kappa(\sigma) = -0.5$  ( $\kappa(\sigma) = 0.5$ ). The homogeneous steady state becomes unstable due to a salt-and-pepper instability (dotted hatching). One of the regimes of pulse suppression is partially covered by the unstable homogeneous steady state region, and so is the regime of multiple pulse generation, indicating that nonlocal feedback control can suppress pulses or generate multiple pulses while destabilizing the homogeneous steady state.

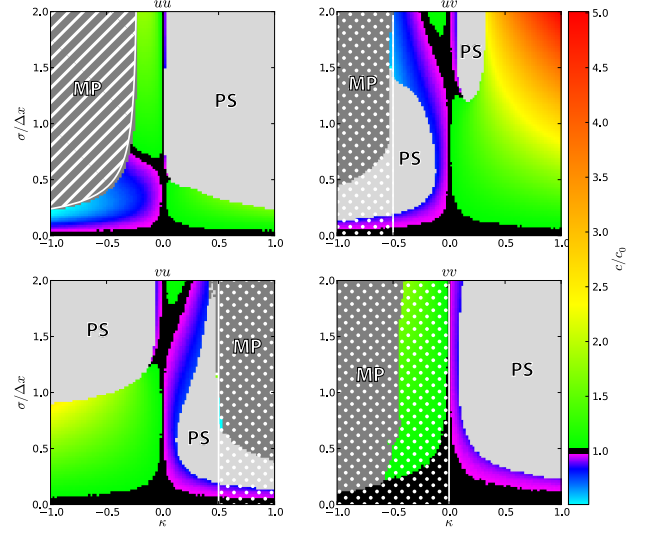


Figure 7: Phase diagrams for four coupling schemes ( $uu$ ,  $uv$ ,  $vu$ ,  $vv$ ) with the  $\delta$ -function integral kernel Eq.(10). Dark gray: Multiple pulse generation (MP). Light gray: Pulse suppression (PS). Colors blue to red: Pulse acceleration or deceleration (the pulse velocity  $c$  normalized by the uncontrolled velocity  $c_0$  is color coded). Black: Pulse speed changes less than 0.5% compared to the uncontrolled pulse. The regions with white hatching indicate an unstable homogeneous steady state due to one of the following instabilities: wave instability (diagonal hatching), Turing instability (vertical hatching), salt-and-pepper instability (dotted hatching). System parameters:  $(\varepsilon, \beta) = (0.08, 1.2)$ .  $L = 600$ , integration timestep  $dt = 0.005$ , spatial resolution  $dx = L/16384 \approx 0.04$ .

In the  $vv$ -coupling scheme pulse suppression is possible only for positive  $\kappa$ . Control configurations with negative control strength  $\kappa$  destabilize the homogeneous steady state by a salt-and-pepper instability, where multiple pulse generation or pulse acceleration are possible.

#### 4.2 Exponential kernel

The phase diagrams for the exponential kernel function (Fig. 8) are qualitatively similar to the ones of the isotropic  $\delta$ -function kernel. Pulse acceleration or deceleration and pulse suppression are found for the same signs of control strength. In the  $uu$ -coupling scheme the border to the regime of multiple pulse generation is, again, well described by the analytically calculated stability boundary of the homogeneous steady state (wave instability). For the  $uv$ - and  $vu$ -coupling scheme the analytical stability boundary of the homogeneous steady state is given by  $\kappa(\sigma) = -1$  and  $\kappa(\sigma) = 1$ , respectively, and a salt-and-pepper instability arises for  $\kappa < -1$  and  $\kappa > 1$ , respectively (outside the range plotted). There are no multiple pulses in the regime shown in the figure. In the  $vv$ -coupling



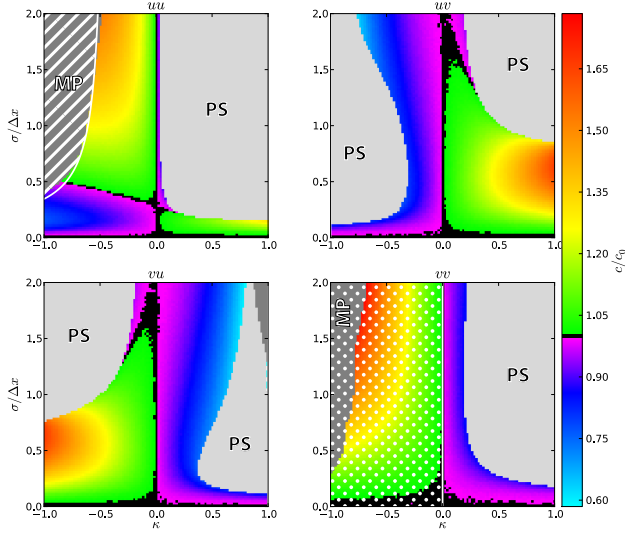


Figure 8: Same as Fig. 7 for the exponential integral kernel Eq.(11).

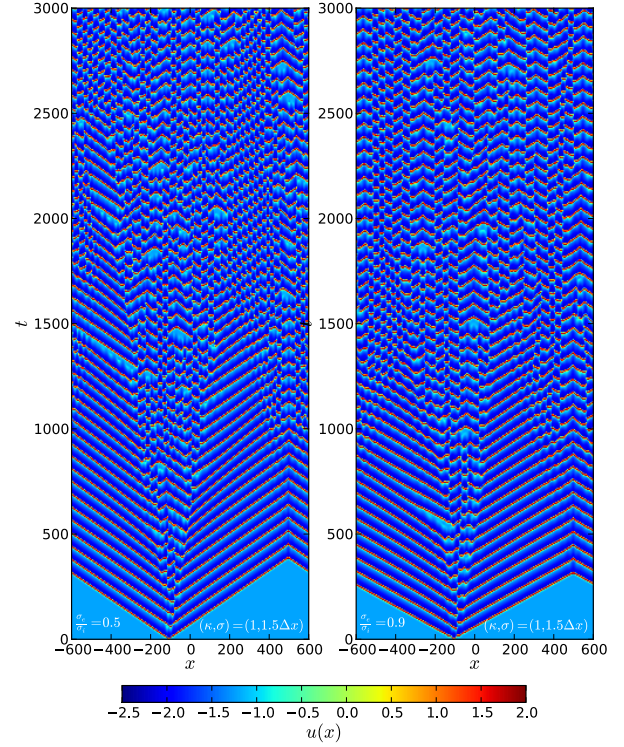


Figure 10: Spatiotemporal plot with the Mexican hat kernel,  $vv$ -coupling-scheme, left:  $r = \sigma_e/\sigma_i = 0.5$ , right:  $r = \sigma_e/\sigma_i = 0.9$ . Other parameters:  $(\kappa, \sigma) = (1, 1.5\Delta x)$ ,  $(\varepsilon, \beta) = (0.08, 1.2)$ ,  $L = 1200$ , integration timestep  $dt = 0.005$ , spatial resolution  $L/16384$ .

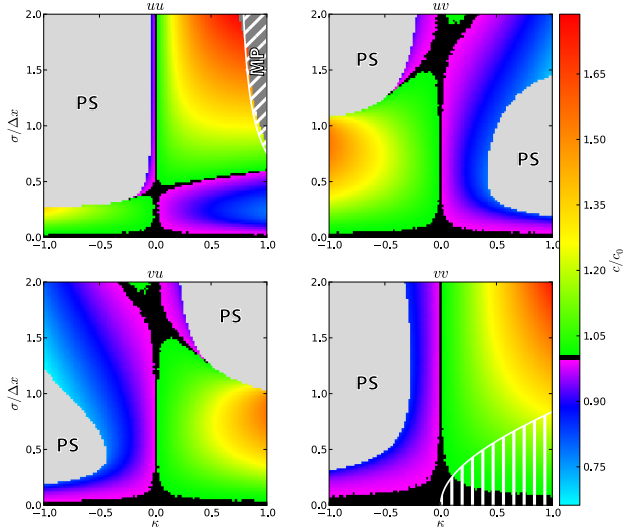


Figure 9: Same as Fig. 7 for the Mexican hat integral kernel Eq.(12) with  $r = \sigma_e/\sigma_i = 0.1$ .

scheme the homogeneous steady state is unstable for  $\kappa < 0$  due to a salt-and-pepper instability, and the pulse acceleration can become much stronger than for the  $\delta$ -function kernel.

### 4.3 Mexican hat kernel

The Mexican hat kernel (Fig. 9) differs from the other kernels. First of all, the term  $\eta U(x)$  vanishes, as  $\eta = 0$ .

Second, the second moment of the kernel

$$M_2 = \frac{1}{2} \int_{-\infty}^{\infty} y^2 \ker(y) dy$$

is negative while it is positive for the other kernel functions. This is the reason why the phase diagrams are qualitatively similar as for the previous kernels if  $\kappa$  is replaced by  $-\kappa$ : The regimes of pulse suppression are found for negative coupling strength  $\kappa$  in the self-coupling schemes  $uu$  and  $vv$ , and on the opposite sides of  $\kappa$  in the cross-coupling schemes, compared to the other kernels, and the same holds for acceleration and deceleration of pulses. It should be noted that the instabilities of the homogeneous steady state in the  $vv$ -coupling scheme are of Turing type for the Mexican hat kernel, whereas they are of the salt-and-pepper type for the other kernels. Turing instabilities also arise in the  $uv$ -coupling scheme for  $\kappa(\sigma) > 1.689$  ( $r = 0.1$ ),  $> 1.366$  ( $r = 0.5$ ),  $> 1.317$  ( $r = 0.9$ ), and in the  $vu$ -coupling scheme for negative  $\kappa(\sigma)$  smaller than the corresponding negative threshold values. In the  $uu$ -coupling scheme interesting spatiotemporal patterns are observed in the regime of multiple pulse generation that is not overlapping with an unstable homogeneous steady state. An exemplary plot is provided in Fig. 10.

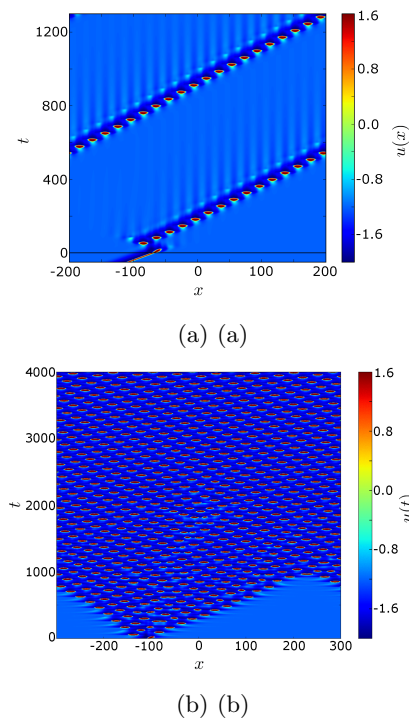


Figure 11: Spatiotemporal plots of complex space time patterns. The initial condition is the stable pulse of the uncontrolled system. (a) Blinking traveling pulse: Isotropic  $\delta$ -function,  $vu$ -coupling scheme,  $(\kappa, \sigma) = (0.48, 1.16\Delta x)$ . (b) Blinking traveling wave. Control configuration: exponential function,  $vu$ -coupling scheme,  $(\kappa, \sigma) = (0.98, 1.98\Delta x)$ . Parameters:  $(\varepsilon, \beta) = (0.08, 1.2)$ .

#### 4.4 Complex spatio-temporal patterns

In our simulations we have also observed more complex spatiotemporal patterns. In general, these occur for parameter values close to the boundary of the multiple pulse regime. Figure 11 shows examples of spatiotemporal plots of a blinking traveling pulse (a) and a blinking traveling wave (b). It appears that they might be due to the interaction of Hopf and wave instabilities.

## 5 Discussion

It has been shown that nonlocal control is able to accelerate, decelerate, and suppress an initially stable traveling pulse for various choices of the integral kernels and coupling schemes. Nonlocal control is also able to generate space-time patterns not present without control, e.g., Turing patterns and wave patterns, or even more complex patterns like salt-and-pepper instabilities or blinking pulses and waves. The control term can destabilize the homogeneous steady state in certain control parameter regimes. The boundaries of these instability regimes have been analytically described.

In detail we have considered an isotropic  $\delta$ -function kernel, an exponential kernel, and a Mexican hat kernel,

which combines short range activation with long range inhibition, and is thus of particular relevance for neuronal systems. As coupling schemes we have used diagonal (activator-activator or inhibitor-inhibitor) and non-diagonal (activator-inhibitor or inhibitor-activator) coupling. Activator self-coupling always gives rise to wave instabilities for the parameters investigated. The cross-coupling schemes and the inhibitor self-coupling scheme can cause Turing instabilities when using the Mexican hat control kernel, and salt-and-pepper instabilities when using the isotropic  $\delta$ -function or the exponential function. The spatial period of wave trains and Turing patterns can be tuned by changing the spatial coupling range of the control kernel.

The linear stability analysis of the homogeneous steady state also enables one to classify the type of the emerging instability as Turing, wave, or salt-and pepper instability. The analytical predictions for the stability boundaries of the homogeneous steady state are in good agreement with the simulation results of the nonlinear system. In the activator self-coupling scheme, the boundary of the regime of multiple pulse generation coincides precisely with the analytically calculated stability boundary of the homogeneous steady state. Care must, however, be taken for the other coupling schemes. There are control configurations that suppress or support stable pulses in the first place, but will eventually after long transient times destabilize the homogeneous steady state leading to the generation of pulses. Therefore in simulations sufficiently long simulation times must be used.

## Acknowledgment

This work was supported by DFG in the framework of SFB 910 “Control of self-organizing nonlinear systems”. Helpful discussions with Julien Siebert are gratefully acknowledged.

## References

1. Daniel M. Abrams and S. H. Strogatz. Chimera states for coupled oscillators. *Phys. Rev. Lett.*, 93(17):174102, 2004.
2. C. A. Bachmair. Nonlocal control of pulse propagation in excitable media, 2013. Master’s Thesis, TU Berlin.
3. M. Bär, M. Falcke, M. Hildebrand, M. Neufeld, H. Engel, and M. Eiswirth. Chemical turbulence and standing waves in a surface reaction model: The influence of global coupling and wave instabilities. *Int. J. Bifur. Chaos*, 4:499, 1994.
4. B. N. Belintsev, M. A. Livshits, and M. V. Volkenstein. Pattern formation in systems with nonlocal interactions. *Z. Phys. B*, 44(4):345–351, 1981.
5. C. Beta, M. G. Moula, A. S. Mikhailov, H. H. Rotermund, and G. Ertl. Excitable CO oxidation on Pt(110) under nonuniform coupling. *Phys. Rev. Lett.*, 93(18):188302, 2004.
6. G. Bordyugov and H. Engel. Creating bound states in excitable media by means of nonlocal coupling. *Phys. Rev. E*, 74:016205, 2006.



7. J. Christoph and M. Eiswirth. Theory of electrochemical pattern formation. *Chaos*, 12(1), 2002.
8. P. Colet, Manuel A. Matías, L. Gelens, and D. Gomila. Formation of localized structures in bistable systems through nonlocal spatial coupling I: General framework. *Phys. Rev. E*, 89(1):012914, 2014. arXiv:1305.6801v1.
9. R. V. Craster and R. Sassi. Spectral algorithms for reaction-diffusion equations. *Technical Report*, 99, 2006.
10. M. A. Dahlem, R. Graf, A. J. Strong, J. P. Dreier, Y. A. Dahlem, M. Sieber, W. Hanke, K. Podoll, and E. Schöll. Two-dimensional wave patterns of spreading depolarization: retracting, re-entrant, and stationary waves. *Physica D*, 239:889–903, 2010.
11. M. A. Dahlem and T. M. Isele. Transient localized wave patterns and their application to migraine. *J. Math. Neurosci.*, 3:7, 2013.
12. M. A. Dahlem, F. M. Schneider, and E. Schöll. Failure of feedback as a putative common mechanism of spreading depolarizations in migraine and stroke. *Chaos*, 18:026110, 2008.
13. J. P. Dreier. The role of spreading depression, spreading depolarization and spreading ischemia in neurological disease. *Nat. Med.*, 17:439–447, 2011.
14. R. FitzHugh. Impulses and physiological states in theoretical models of nerve membrane. *Biophys. J.*, 1:445–466, 1961.
15. L. Gelens, Manuel A. Matías, D. Gomila, Tom Dorissen, and P. Colet. Formation of localized structures in bistable systems through nonlocal spatial coupling. II. the nonlocal ginzburg-landau equation. *Phys. Rev. E*, 89(1):012915, 2014.
16. A. M. Hagerstrom, Thomas E. Murphy, R. Roy, P. Hövel, I. Omelchenko, and E. Schöll. Experimental observation of chimeras in coupled-map lattices. *Nature Physics*, 8:658–661, 2012.
17. H. Haken. *Synergetics, An Introduction*. Springer, Berlin, 3 edition, 1983.
18. M. Hildebrand, H. Skødt, and K. Showalter. Spatial symmetry breaking in the belousov-zhabotinsky reaction with light-induced remote communication. *Phys. Rev. Lett.*, 87(8):088303, 2001.
19. Kukjin Kang, Michael Shelley, and H. Sompolsinsky. Mexican hats and pinwheels in visual cortex. *PNAS*, 100(5):2848–2853, 2002.
20. Raymond Kapral and K. Showalter, editors. *Chemical Waves and Patterns*. Kluwer, Dordrecht, 1995.
21. H. Karatas, S. E. Erdener, Y. Gursoy-Ozdemir, S. Lule, E. Eren-Kocak, Z. D. Sen, and T. Dalkara. Spreading depression triggers headache by activating neuronal Panx1 channels. *Science*, 339(6123):1092–1095, 2013.
22. J. P. Keener and J. Sneyd. *Mathematical physiology*. Springer, New York, Berlin, 1998.
23. Y. Khazan and L. M. Pismen. Differential flow induced chemical instability on a rotating disk. *Phys. Rev. Lett.*, 75:4318–4321, 1995.
24. F. Kneer, E. Schöll, and M. A. Dahlem. Nucleation of reaction-diffusion waves on curved surfaces. *New J. Phys.*, 16:053010, 2014.
25. Shigeru Kondo and Takashi Miura. Reaction-diffusion model as a framework for understanding biological pattern formation. *Science*, 329(5999):1616–1620, 2010.
26. Y. Kuramoto. *Chemical Oscillations, Waves and Turbulence*. Springer-Verlag, Berlin, 1984.
27. Y. Kuramoto and D. Battogtokh. Coexistence of Coherence and Incoherence in Nonlocally Coupled Phase Oscillators. *Nonlin. Phen. in Complex Sys.*, 5(4):380–385, 2002.
28. Y. J. Li, Julia Oslonovitch, N. Mazouz, F. Plenge, K. Krischer, and Gerhard Ertl. Turing-type patterns on electrode surfaces. *Science*, 291(5512):2395–2398, 2001.
29. B. Lindner, J. García-Ojalvo, A. B. Neiman, and L. Schimansky-Geier. Effects of noise in excitable systems. *Phys. Rep.*, 392:321–424, 2004.
30. J. Löber, R. Coles, J. Siebert, H. Engel, and E. Schöll. Control of chemical wave propagation. In A. S. Mikhailov and G. Ertl, editors, *Engineering of Chemical Complexity II*. World Scientific, Singapore, 2014. arXiv:1403.3363.
31. H. Malchow. Nonlinear plankton dynamics and pattern formation in an ecohydrodynamic model system. *Journal of Marine Systems*, 7(2&4):193–202, 1996. The Coastal Ocean in a Global Change Perspective.
32. Erik A. Martens, Shashi Thutupalli, Antoine Fourrière, and Oskar Hallatschek. Chimera states in mechanical oscillator networks. *Proc. Nat. Acad. Sciences*, 110:10563, 2013.
33. N. Mazouz, G. Flätgen, and K. Krischer. Tuning the range of spatial coupling in electrochemical systems: From local via nonlocal to global coupling. *Phys. Rev. E*, 55:2260, 1997.
34. M. Meixner, A. De Wit, S. Bose, and E. Schöll. Generic spatio-temporal dynamics near Turing-Hopf codimension-two bifurcations. *Phys. Rev. E*, 55:6690, 1997.
35. M. Meixner, P. Rodin, E. Schöll, and A. Wacker. Lateral current density fronts in globally coupled bistable semiconductors with S- or Z-shaped current voltage characteristic. *Eur. Phys. J. B*, 13:157, 2000.
36. U. Middy, M. Sheintuch, M. D. Graham, and D. Luss. Patterns of temperature pulses on electrically heated catalytic ribbons. *Physica D*, 63:393–409, 1992.
37. A. S. Mikhailov. *Foundations of Synergetics Vol. I*. Springer, Berlin, 2 edition, 1994.
38. A. S. Mikhailov and K. Showalter. Control of waves, patterns and turbulence in chemical systems. *Phys. Rep.*, 425:79–194, 2006.
39. J. Nagumo, S. Arimoto, and S. Yoshizawa. An active pulse transmission line simulating nerve axon. *Proc. IRE*, 50:2061–2070, 1962.
40. Ernesto M. Nicola, M. Bär, and H. Engel. Wave instability induced by nonlocal spatial coupling in a model of the light-sensitive belousov-zhabotinsky reaction. *Phys. Rev. E*, 73(6):066225, 2006.
41. Ernesto M. Nicola, M. Or-Guil, Wilfried Wolf, and M. Bär. Drifting pattern domains in a reaction-diffusion system with nonlocal coupling. *Phys. Rev. E*, 65, 2002.
42. I. Omelchenko, Oleh E. Omel’chenko, P. Hövel, and E. Schöll. When Nonlocal Coupling Between Oscillators Becomes Stronger: Patched Synchrony or Multichimera States. *Phys. Rev. Lett.*, 110:224101, 2013.
43. V. Petrov, M. J. Crowley, and K. Showalter. Tracking unstable periodic orbits in the belousov-zhabotinsky reaction. *Phys. Rev. Lett.*, 72:2955, 1994.
44. L. M. Pismen. *Patterns and Interfaces in Dissipative Dynamics*. Springer Series in Synergetics. Springer, Berlin, 2006.
45. F. Plenge, P. Rodin, E. Schöll, and K. Krischer. Breathing current domains in globally coupled electrochemical systems: A comparison with a semiconductor model. *Phys. Rev. E*, 64:056229, 2001.

46. A. Rovinsky and M. Menzinger. Chemical instability induced by a differential flow. ii: Experiments. *Phys. Rev. Lett.*, 70(778), 1993.
47. F. M. Schneider, E. Schöll, and M. A. Dahlem. Controlling the onset of traveling pulses in excitable media by nonlocal spatial coupling and time delayed feedback. *Chaos*, 19:015110, 2009.
48. E. Schöll. *Nonlinear spatio-temporal dynamics and chaos in semiconductors*. Cambridge University Press, Cambridge, 2001. Nonlinear Science Series, Vol. 10.
49. M. Sheintuch and O. Nekhamkina. Reaction-diffusion patterns on a disk or a square in a model with long-range interaction. *J. Chem. Phys.*, 107(19):8165–8174, 1997.
50. Shin-ichiro Shima and Y. Kuramoto. Rotating spiral waves with phase-randomized core in nonlocally coupled oscillators. *Phys. Rev. E*, 69(3):036213, 2004.
51. J. Siebert, S. Alonso, M. Bär, and E. Schöll. Dynamics of reaction-diffusion patterns controlled by asymmetric nonlocal coupling as limiting case of differential advection. *Phys. Rev. E*, 89(5):052909, 2014.
52. Dan Tanaka and Yoshiki Kuramoto. Complex ginzburg-landau equation with nonlocal coupling. *Phys. Rev. E*, 68(2):026219, 2003.
53. M. R. Tinsley, Simbarashe Nkomo, and K. Showalter. Chimera and phase cluster states in populations of coupled chemical oscillators. *Nature Physics*, 8:662–665, 2012.
54. H. Varela, C. Beta, A. Bonnefont, and K. Krischer. Transitions to electrochemical turbulence. *Phys. Rev. Lett.*, 94(174104), 2005.
55. J. von Hardenberg, E. Meron, M. Shachak, and Y. Zarmi. Diversity of vegetation patterns and desertification. *Phys. Rev. Lett.*, 87:198101, 2001.
56. Xiaoming Xu, William Bosking, Gyula Sárosi, James Stefanski, Daniel Shima, and Vivien Casagrande. Functional organization of visual cortex in the owl monkey. *J. Neurosci.*, 24(28):6237–6247, 2004.
57. Arik Yochelis and M. Sheintuch. Drifting solitary waves in a reaction-diffusion medium with differential advection. *Phys. Rev. E*, 81(2):025203, 2010.
58. A. Zakharova, M. Kapeller, and E. Schöll. Chimera death: Symmetry breaking in dynamical networks. *Phys. Rev. Lett.*, 112:154101, 2014.